Applied Radiation and Isotopes 204 (2024) 111120

Contents lists available at ScienceDirect

Applied Radiation and Isotopes

journal homepage: www.elsevier.com/locate/apradiso

TCAD simulations of internal amplification in high purity germanium detectors

D. Maneuski [a,*], V. Gostilo [b]

[a] SUPA School of Physics and Astronomy, University of Glasgow, Kelvin Building, University Avenue, Glasgow, G12 8QQ, UK
[b] Baltic Scientific Instruments Ltd, Ramulu 3, Riga, LV-1005, Latvia

ARTICLE INFO

Keywords:
Semiconductor detectors
Solid state detectors
HPGe detectors
Internal amplification
Charge transport and multiplication
Detector modelling and simulations

ABSTRACT

Simulations of internal amplification processes in high purity germanium (HPGe) detectors for gamma radiation are presented. The Synopsys Sentaurus Technology Computer-Aided Design (TCAD) package was employed to study conditions favourable to charge multiplication within volume of the detector. The physics model was developed, and validated where possible against known results from existing literature. The model was then applied to a new detector and a systematic study of the measurable parameters influencing charge collection and electric field profile was performed. Evidence of the internal amplification in the developed HPGe detector model was demonstrated at 4 kV bias voltage with anode diameter below 100 μm, corresponding to 16 kV/cm electric field and when an additional dopant with concentrations $> 5 \times 10^{10}$ cm^{-3} under the anode implanted. These effects were also simulated and observed in silicon detectors, giving additional confidence in the validity of the findings for germanium, presented in this work.

1. Introduction

A significant number of modern international scientific experiments in the field of fundamental physics are associated with the search of rare events accompanied by the emission of gamma radiation. Such experiments include but are not limited to double beta decay, dark matter searches and neutrino detection. These experiments directly depend on how accurately said rare events can be extracted from a large number of background (false) events which leads to sources of error in their results (Prakash, 2012; Formaggio and Martoff, 2004; Bahcall et al., 2001; Laubenstein et al., 2004; Gilchriese et al., 2023). This imposes strict requirements on almost all of the characteristics of the equipment used in such experiments, especially on its background performance.

HPGe detectors, with their superior energy resolution and high detection efficiency of gamma radiation, are leaders in ultra low background applications (Laubenstein et al., 2004; Gilchriese et al., 2023). However, they do not completely satisfy the experimental requirements. The disadvantage of HPGe detectors is their rather high noise threshold of 2–10 keV associated with: the leakage current, electronics and microphone noise; the reduction of which requires considerable effort (Pullia et al., 2008; Deng et al., 2018).

It has been proposed previously (Starostin and Beda, 2000), that one can effectively reduce the noise threshold of HPGe detectors by means of internal proportional amplification of the signal. The design of such a HPGe detector with internal amplification was described, and guidelines for the detector development were also formed. In 2012, Baltic Scientific Instruments (BSI), together with the Institute of Theoretical and Experimental Physics (ITEPh, Moscow), developed a prototype of a HPGe detector with internal amplification in accordance with the recommendations detailed in Starostin and Beda (2000). However, the investigation into the avalanche processes in the developed detector were ambiguous. Further experiments were suspended until new possible solutions matured.

Internal proportional signal amplification in semiconductor detectors is well studied and implemented in silicon avalanche photodiodes (APDs) (Pansart, 1997; Farrell et al., 1997). There gain of ~10^2–10^4 is achieved by avalanche multiplication of electrons in an electric field (5–6×10^5 V/cm) in a narrow p–n junction with a sensitive volume of several mm^3. The multiplication processes in electronics grade germanium have also been studied and are used in germanium photodiodes (Kang et al., 2009; Michel et al., 2010). However, the characteristics of materials in electronic photodiodes and semiconductor gamma-ray detectors are drastically different. In addition, the size of the region in which the multiplication processes should develop in these devices also significantly differ. These two major factors are likely to determine why carrier multiplication processes have not yet been implemented in detector structures made from ultra high purity germanium (Knoll, 2000; Lutz, 1999).

* Corresponding author.
E-mail address: dima.maneuski@glasgow.ac.uk (D. Maneuski).

https://doi.org/10.1016/j.apradiso.2023.111120
Received 20 April 2023; Received in revised form 14 November 2023; Accepted 20 November 2023
Available online 22 November 2023

The concept of a HPGe detector utilising internal charge amplification for the charge carriers created by the ionisation of impurities is considered to be a promising technology for the detection of dark matter. The investigation of physics mechanisms of the signal formation, charge generation, internal charge amplification, led to a strip structure design for a HPGe detector at liquid helium temperature (~4 K) (Mei et al., 2018). However, the authors left implementation and characterisation of this conceptual design for their future work. Recently, BSI resumed the development and fabrication of a prototype HPGe detector with internal amplification which should operate at optimal temperatures for HPGe detectors ~80 K as conceptualised by Starostin and Beda (2000).

In recent years, numerical simulations became a powerful and effective tool which greatly facilitate the process of finding the right direction for development and affirm or invalidate a proof of concept even before the prototype of the device is fabricated. It is also important that computer simulations significantly reduce the volume of prototypes produced and the need for laborious study of their properties. This makes it expedient to carry out simulations of the detector structures and the processes that should be implemented in the future prototypes.

This work focuses on numerical simulations of carrier multiplication processes in high purity germanium, and studies the conditions for which this multiplication occurs. The aim of this study is to develop novel HPGe detectors of gamma radiation with avalanche multiplication for ultra low-background applications.

2. Materials and methods

2.1. Simulation package and model development implications

The Synopsys Sentaurus TCAD (Synopsys, 2023) finite element simulation package was used to develop the simulation model and conduct calculations. *Sentaurus Device Editor* was employed to build the detector geometry. Static electrical and transient simulations were performed in *Sentaurus Device*. *INSPECT* and *Sentaurus Visual* were used as visualisation tools for data extraction. The simulation project was managed in *Sentaurus Workbench*. A number of Synopsys Sentaurus TCAD limitations related to this study were taken into account while conducting these simulations. Sentaurus physics models are mainly silicon specific. They do not have all parameters defined for the detector grade HPGe. Transient simulations (charge transport in the material) are limited to a single particle interaction only, hence a spectrum from a simulated detector cannot be built as in a Monte Carlo simulation. Alpha particles and heavy ions are the only available charge generation mechanism. Hence additional steps are needed to realistically represent the charge cloud generated in the HPGe detector in order to simulate an X-ray interaction.

2.2. Simulation model description

The bulk material is made of a p-type HPGe with a collecting point anode in the middle of the top surface. The anode is surrounded by a guard ring to reduce the surface leakage current. The cathode is located at the bottom surface of the detector, taking up the entire surface. For all simulations, the bias voltage was applied at the cathode, while anode was kept at 0 V potential, where the charge was collected. Fig. 1 shows the basic detector model geometry. The initial geometry is chosen such to represent a typical detector die manufactured at BSI. A 2D model is sufficient to study the properties of the detector qualitatively. All electric field profile figures presented in this work are drawn along the cut line in the middle of the detector.

For simulation of impurities and doping profiles boron was used as standard acceptor impurity and phosphorus is used to simulate donor impurities (Renker and Lorenz, 2009; Pellegrini et al., 2016; Schlesinger and James, 1995; Owens, 2019). Boron and phosphorus

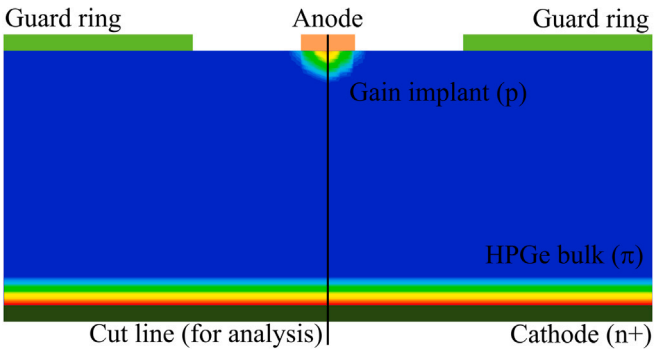

Fig. 1. TCAD HPGe detector model geometry (not to scale). The detector is represented by a 2D model, 20 mm thickness, 41 mm diameter. Guard rings are 2.5 mm wide spanning to the edge of the top surface. Anode diameter is varied between 50 and 2000 μm. Cathode covers the bottom of the detector.

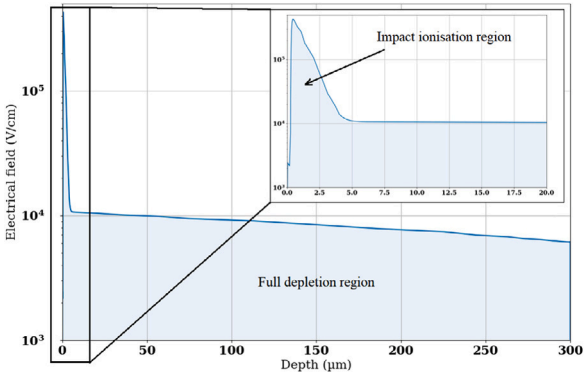

Fig. 2. Simulated electric field profile across a silicon LGAD detector. Electric field reaches theoretical levels for impact ionisation to arise. Impact ionisation occurs in the first 5 μm.

are the standard impurity and profile concentrations for simulations in Sentaurus TCAD.

Default net carrier concentration of the bulk is assumed 5×10^{9} cm^{-3}, which is typical for these devices (Renker and Lorenz, 2009). The detector has planar cylinder configuration, diameter D = 41.0 mm, height H = 20.0 mm. The guard ring, made of an Aluminium contact placed directly on bulk material, was grounded at all times. The cathode is *n*+ type, doped with phosphorus, placed under an Indium contact. The node is represented by an Aluminium contact placed directly on top of the gain implant. All simulations were performed at 77 K, which is the boiling temperature of liquid nitrogen (standard operating temperature of most HPGe detectors). The mobility of carriers was altered such as to achieve mobilities known from existing literature at 77 K (38600 $cm^2V^{-1}s^{-1}$ (Bruyneel, 2006)). The simulated values obtained are 39000 $cm^2V^{-1}s^{-1}$ and 42000 $cm^2V^{-1}s^{-1}$ for electrons and holes respectively. The lifetime for electrons was set to 4.5×10^{-4} s (Fan et al., 1954).

The injected charge profile was adapted from Maneuski et al. (2020) to be the equivalent of a 75 keV photon (4.1 fC in Ge) interacting at a 5 mm distance from the anode in the middle of the detector.

2.3. Simulation model validation

Before simulations of the HPGe detector prototype could be conducted, it was essential to validate the model against known results. Since there are no similar TCAD simulation results for HPGe available in the literature, the model was validated on a generic silicon detector, in which the processes of avalanche multiplication have been observed and extensively studied.

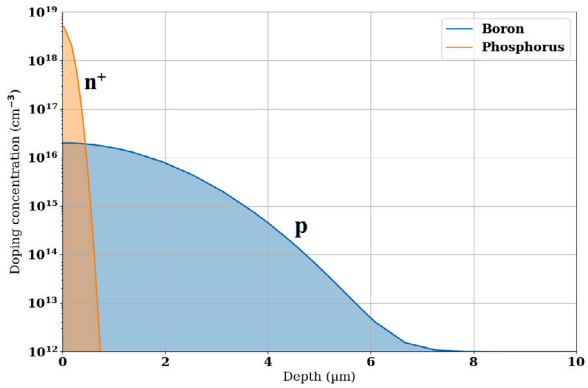

Fig. 3. Simulated doping profile across a silicon LGAD detector. To control the gain, one must control the boron concentration at the junction between the n^+ and p implants.

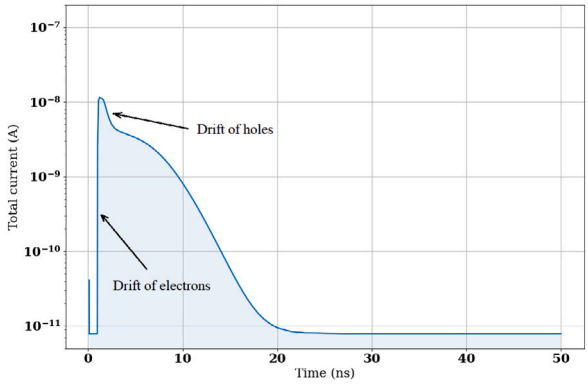

Fig. 4. Simulated change collection profile for a typical planar silicon PIN detector. Electrons are collected first. Then an induced holes signal can be observed. Note a lower leakage current compared to a response from an LGAD detector in Fig. 5.

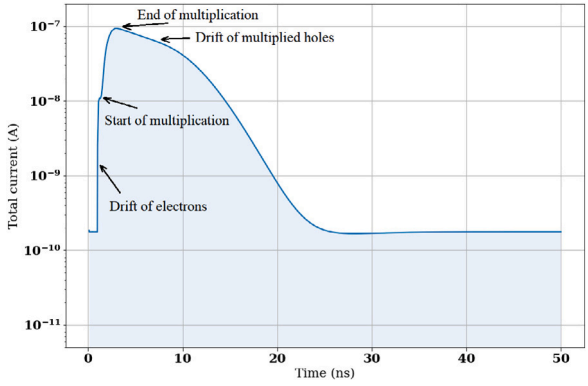

Fig. 5. Simulated change collection profile for a typical silicon LGAD detector. When electron charge is collected, this is followed by additional change being generated due to impact ionisation. Then an induced holes signal can be observed.

There are two classes of devices developed over the years which employ internal gain namely Single Photon Avalanche Detectors (SPADs), (Renker and Lorenz, 2009) and Low Gain Avalanche Diodes (LGADs) (Pellegrini et al., 2016). Typically, SPADs have gain of $\sim 10^6$, while LGADs gain ranges between 3 and 50.

Fig. 2 shows simulated electric field profile of a generic LGAD device using the developed physics model but adapted for silicon. A high strength field region is observed close to the anode of the device.

Table 1
HPGe simulation model study parameter space.

Fixed parameters	Variable parameters	Range
Geometry	Bias voltage	100–4000 V
Temperature	Anode diameter	50–2000 μm
Carrier mobility and life time	Bulk doping	0–5e15 cm^{-3}
Cathode doping profile shape	Cathode doping	0–4e18 cm^{-3}
Injected charge	Anode doping	0–5e18 cm^{-3}

Impact ionisation occurs in the region, leading to charge multiplication. The electric field strength required to generate impact ionisation is $\sim 5 \times 10^5$ V/cm (Starostin and Beda, 2000). Fig. 3 shows the corresponding doping concentration through the n-type electrode and p-type multiplication implant.

Figs. 4 and 5 compare charge collection profiles for a reference PIN diode and a corresponding LGAD device using the developed model adapted for silicon. In the PIN diode the electrons are collected quickly at the anode while the holes drift slowly through the device and are collected at the cathode. In the LGAD device the signal height is several times higher while additional features are observed. These features form the hypothesis for evidence of multiplication in HPGe simulations presented later in this work.

The developed model yielded results in a silicon detector which align well with simulations and experimental measurements from devices in literature (see e.g. Moffat (2020) and references therein). Hence, it is hypothesised this model can be applied to an HPGe detector with limitations described in Sections 2.1 and 2.2.

2.4. Simulation parameter space

Simulations of an HPGe detector were performed in sequence. Well known parameters were fixed at given predefined or optimised values, while other parameters were subsequently varied one at a time to yield an optimal performance of the detector. A summary of the parameters studied are shown in Table 1. In the initial stage the geometry, temperature, injected charge, carrier mobility and life time were fixed. Cathode doping profile was optimised according to literature (see Section 3.1) and was kept unchanged for the subsequent simulations. The parameters to be optimised are: applied detector bias voltage, anode diameter, concentration of acceptor carriers in the bulk, cathode and finally anode. The varied parameters can be set during the fabrication or operation of the detector.

Simulations were run to determine the maximum electric field near the collecting anode and seek evidence of multiplication in the current profile (similar to the LGAD device profiles as explained in Section 2.3)

3. Results and discussion

3.1. Tuning of the cathode doping profile shape

HPGe detector cathodes are normally manufactured by the diffusion of lithium into a germanium bulk. The diffusion profiles of lithium into the HPGe detector cathodes manufactured at BSI were measured and a fit produced (Pratt and Friedman, 1966). In this study the diffusion parameters were tuned such that the observed diffusion profile matched that reported fit. Fig. 6 shows the overlaying of the simulated results with data and the fit from Pratt and Friedman (1966).

To match the simulated data to the fit, following variables were tuned: the maximum concentration of dopants at the surface of the detector; the shape and length of the diffusion profile; and end-point concentration. The optimised profile achieved as a result of the simulations is consistent with the fit shown in Fig. 6 to within 10%.

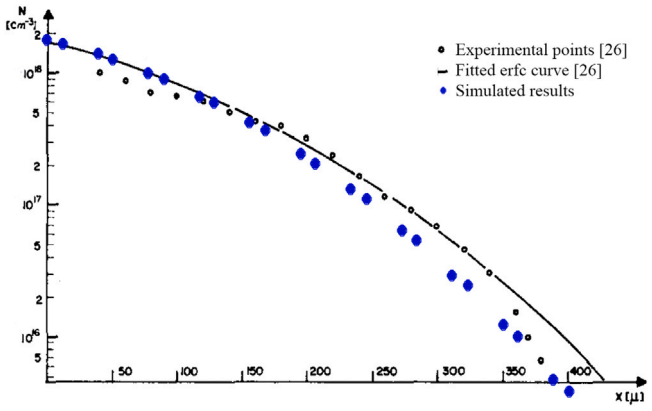

Fig. 6. Diffusion of lithium into germanium. Overlaid data (large solid blue dots) is simulation results from this study.
Source: Adapted from Figure 2 in *Pratt et al. 1966* (Pratt and Friedman, 1966).

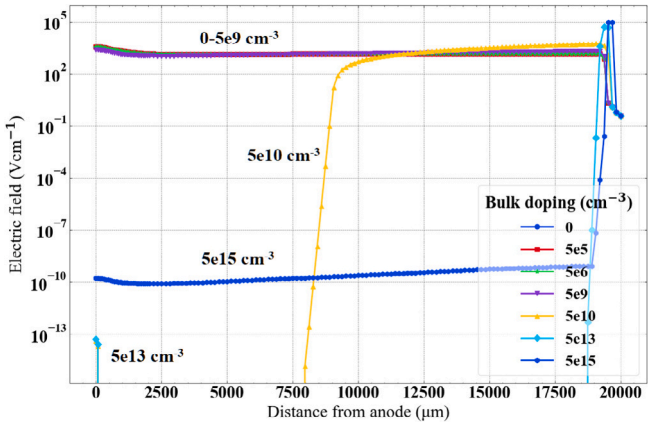

Fig. 7. Electric field profiles for various bulk net carrier concentrations represented by boron impurities. Experimentally measured concentration of 5e9 cm^{-3} and below results in an electric field across the entire volume of the detector. Higher concentrations of impurities are manifested by lack of electric field. In this simulation: bias voltage = 3 kV, anode diameter = 1000 μm, cathode doping = 4e18 cm^{-3}.

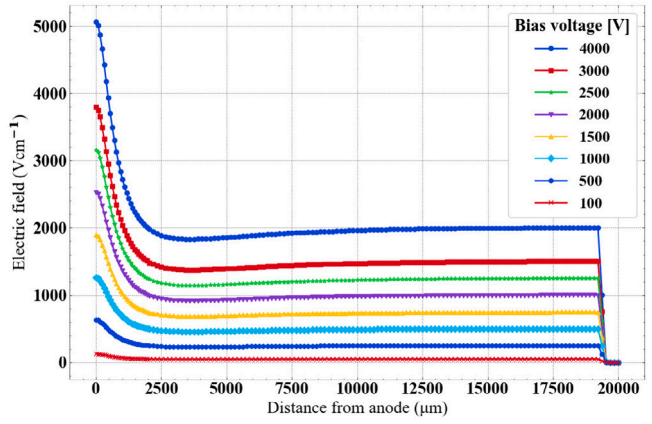

Fig. 8. Electric field profiles for various bias voltages. Empirically, electric field inside the detector volume should be proportional to the applied bias voltage. This is confirmed by the simulation and qualified for the studied detector geometry. At maximum bias voltage of 4 kV strongest electric field in the vicinity of anode reaches 5 kV/cm. In this simulation: anode diameter = 1000 μm, bulk doping = 0 cm^{-3}, cathode doping = 4e18 cm^{-3}.

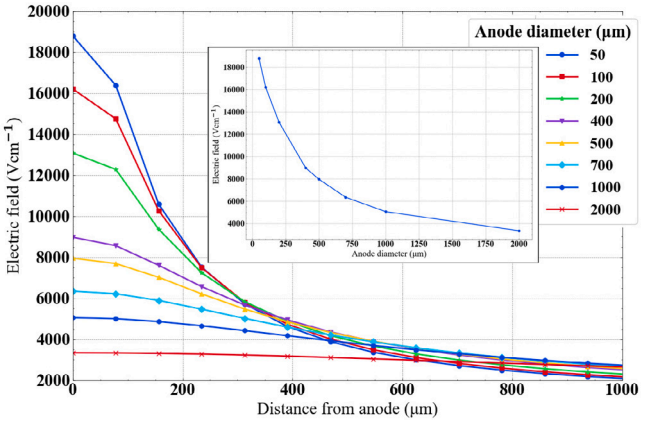

Fig. 9. Electric field profiles through the bulk of the detector. A higher electric field can be achieved with a smaller anode diameter. The insert shows the strength of the electric field at the surface of the anode as a function of anode diameter. In this simulation: bias voltage = 3 kV, bulk doping = 0 cm^{-3}, cathode doping = 4e18 cm^{-3}.

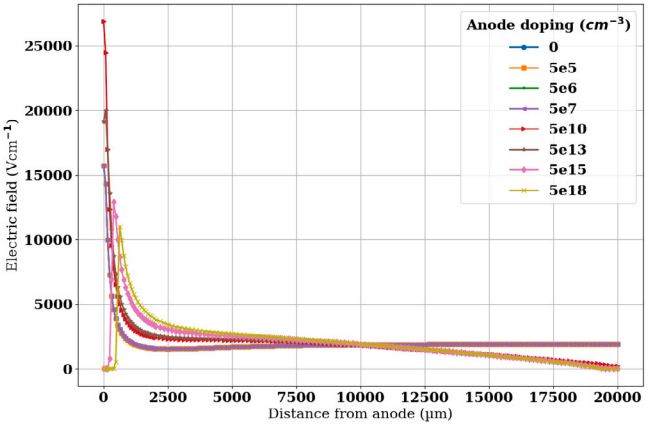

Fig. 10. Electric field profiles for different anode doping concentrations. Two distinct groups of profiles can be observed: < 5e10 cm^{-3} — the electric field behaves similar to the case with no anode doping; > 5e10 cm^{-3} — the electric field profiles are similar to those of a silicon detector with internal signal amplification. In this simulation: bias voltage = 4 kV, anode diameter = 100 μm, bulk doping = 0 cm^{-3}, cathode doping = 4e18 cm^{-3}.

3.2. Bulk doping concentration variation

The net carrier concentration in the bulk of the detector is a known parameter. However, due to limitations of the physics available in the TCAD simulation package, it is necessary to validate simulated values against the net carrier concentration represented by *BoronActiveConcentration* parameter in the model. Fig. 7 shows the electric field profiles simulated at different bulk carrier concentrations. The default experimentally measured concentration value for HPGe material is 5×10^9 cm^{-3}. The electric field at the anode is 2.5×10^3 V/cm, while spanning between $1{\times}10^3$ and $2{\times}10^3$ V/cm throughout the volume of the detector. This indicates that *BoronActiveConcentration* parameter gives adequate representation as the type of carriers in the bulk. Additional simulations were performed to assess the sensitivity of the parameter. Results indicate that reducing the net carrier concentration enhances electric field through the detector volume and is hence favourable for charge collection. In fabrication setting this requires the highest purity germanium available to manufacture those devices from. Hence, this requirement could impose significant limitations on practical possibility of fabricating a detector with internal amplification.

3.3. Bias voltage variation

The strength of the electric field inside the detector should be proportional to the applied bias voltage. In this simulation this dependence is quantified by applying a range of bias voltages used in the realistic detector operation environments. Fig. 8 depicts the expected behaviour of the electric field profiles. The maximum voltage usually applied to the detector does not exceed 4–5 kV. In this simulation the maximum applied bias voltage was limited to 4 kV. Note that the electric field at the anode of the detector is ∼5 kV/cm. According to calculations, the critical electric field required for avalanche generation is ∼90 kV/cm (Starostin and Beda, 2000). All subsequent simulations vary available fabrication parameters aiming to maximise the strength of the electric field in the vicinity of the anode. In addition to this, the charge collection profile is used as an indicator for evidence of internal multiplication. This simulation conclusively indicates that maximising applied bias voltage leads to stronger electric field in the vicinity of the anode and hence increases the probability of internal multiplication to take place.

3.4. Anode diameter variation

Electric field lines naturally end at the anode and thus funnel charge generated in the bulk here. Hence the anode diameter changes the electric field in its vicinity. A study was conducted to establish the relationship between the anode diameter and strength of the electric field for a given detector geometry. In Fig. 9 a region of up to 1000 μm from the anode of the detector is shown. As can be seen from Fig. 9, the electric field can be increased by a factor of 6 when the anode diameter is reduced from 1000 to 50 μm. This simulation conclusively indicates that higher electric fields are achieved with smaller anode diameters. Hence, the smallest anode diameter achievable at the detector production stage is desirable for the maximum electric field. For example, the electric field of 16 kV/cm can be achieved with a 100 μm anode diameter at 4 kV bias voltage. In practice, conventional photo-lithographic techniques can allow fabrication of anode diameters smaller than that has been simulated here. However, there are at least two limiting factors. Firstly, wire-bonding gold wire is typically 30 μm diameter, rendering minimal anode diameter to be at least 40 μm (Gostilo et al., 2001, 2002). Secondly, anode border is not effective in multiplying electrons. Those electrons drifting close to the anode border do not go through the gain layer under the anode but rather go at the edge of the anode and therefore are not multiplied. This was demonstrated in Moffat and Bates (2021) for silicon. The effects shown there are not observed in this simulations due to more complicated nature of the model in Moffat and Bates (2021) involving calibrated routines for realistic representation of the fabrication steps by *Sentaurus Process*. Hence, conservative assumptions set lower limit for the anode diameter in order of 100 μm for the HPGe detector.

3.5. Anode doping concentration variation

Internal amplification of the signal can be achieved in silicon detectors by means of an additional highly doped region under the anode (Tapan et al., 1997). Following the same principle, the simulation in this section seeks to establish conditions of internal amplification in HPGe. A region of highly doped acceptor carriers was created under the anode. The doping profile parameters were chosen as to match those of the cathode. The parameters of bulk concentration, bias voltage, anode diameter and cathode doping profile were fixed to their optimal values as determined in previous sections. Two sets of simulations were performed: quasistationary simulations established electric field profiles across the depth of the detector at different anode doping concentrations; and transient simulations of injected charge resulted in current transients at the anode.

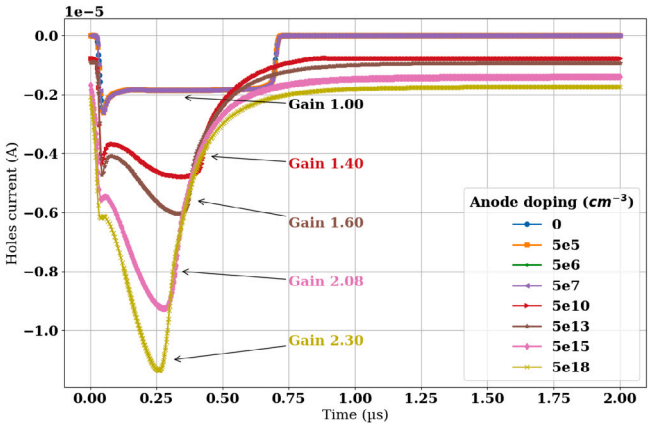

Fig. 11. Holes current at the anode for different anode doping concentrations. Two distinct groups of current profiles can be observed. For doping concentrations > 5e10 cm^{-3} evidence of internal amplification is demonstrated by the secondary rise of the signal after initial signal occurring within the first ∼50 ns. Resulting gain is highlighted for each pulse. In this simulation: bias voltage = 4 kV, anode diameter = 100 μm, bulk doping = 0 cm^{-3}, cathode doping = 4e18 cm^{-3}.

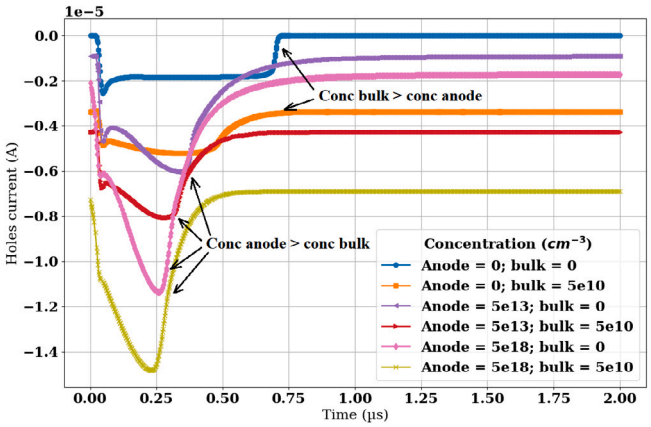

Fig. 12. Holes current at the anode for different combinations of anode and bulk doping concentrations. Internal amplification is observed when anode doping concentration exceeds bulk doping concentration. In this simulation: bias voltage = 4000 V, anode diameter = 100 μm, cathode doping = 4e18 cm^{-3}.

Fig. 10 shows two distinct groups of electric field profiles. For anode doping concentrations below 5×10^{10} cm^{-3}, the electric field behaves similar to the case with no anode doping. For anode doping concentrations above 5×10^{10} cm^{-3}, the electric field profiles are similar to those of a silicon detector with internal signal amplification. In Fig. 11 charge collection at the anode as a function of doping concentration is shown. For anode doping concentrations above 5×10^{10} cm^{-3} current profiles show evidence of internal amplification. After the initial pulse rise which occurs within the first ∼50 ns, there is a secondary rise of the signal observed. This is believed to be attributed to the internal amplification at the anode-bulk interface. The largest (smallest) pulse by amplitude is observed for the simulated anode doping concentration of 5×10^{18} cm^{-3} (5×10^{10} cm^{-3}).

Gain was calculated as a fraction of charge (an integral of the pulse after the leakage current subtraction) normalised to the charge at 0 anode doping. The largest gain observed was 2.3 at the highest simulated anode doping of 5×10^{18} cm^{-3} while the smallest observable gain of 1.4 was evident at anode doping of 5×10^{10} cm^{-3}.

It is important to point out that internal amplification was observed at electric field amplitudes well below those calculated analytically

in Starostin and Beda (2000). Nevertheless, the simulation results systematically showed the rise of the secondary signal, which is attributed to the avalanche multiplication in the developed detector model.

3.6. Bulk and anode doping concentration variation

This simulation established a qualitative relationship between the bulk and anode doping concentrations. A two-dimensional simulation of a bulk-anode doping parameter space was performed. Fig. 12 summarises key current profile plots. As the bulk doping concentration rises, so does the baseline of the detector response. This, in a real setting, translates into a higher leakage current. In the case where the bulk concentration is larger than the anode concentration, internal amplification is either very weak or not present. When the anode doping concentration exceeds that of the bulk concentration, there is observable evidence of internal amplification.

3.7. Anode, cathode and bulk doping concentration variation

The last discussed simulation in this paper looks at the three dimensional variation of all three doping concentrations in the detector: anode, cathode and bulk. This study is performed to document dependencies (if any) between these parameters which were not captured before. The results of this simulation show, that the cathode doping concentration does not influence charge collection at given anode and bulk concentrations. This simulation also confirms results of the previous section. Internal amplification is observed when anode doping concentration exceeds bulk doping concentration.

4. Conclusions

The concept of internal amplification has been successfully demonstrated in a high purity germanium (HPGe) detector, achieving gain factor of up to 2.3 with an additional highly dopped region (up to 5×10^{18} cm^{-3}) under the anode. Simulations were performed using Sentaurus TCAD package.

A model of a HPGe detector was created and validated against known material properties and measured parameters. The overall geometry, temperature, charge carrier properties, cathode doping profile and injected charge were fixed parameters. In the simulations the bias voltage and the anode diameter were variable quantities. The bulk, cathode and anode doping concentrations were varied to establish the conditions at which the electric field was maximised on the anode, and see whether there was evidence of internal amplification in the charge collection profile. Evidence of charge amplification through the collected charge profile under anode with diameter below 100 μm was seen in the simulations at 16 kV/cm electric field strength which was achieved at 4 kV bias voltage. These conditions require, ultra high purity germanium to enhance the electric field through the of bulk of the detector, and an additional doping under the anode in excess of 5×10^{10} cm^{-3}. The simulations show that the doping concentration in the profile has to be several orders of magnitude larger than one in the bulk. This requirement broadly agrees well with conditions of avalanche generation in silicon. The simulations also demonstrated the optimal strategy for anode diameter and biasing conditions required to maximise electric field at the anode.

In general, the obtained simulation results cautiously indicate that internal amplification is possible in HPGe crystals. However, the actual possible characteristics of HPGe detectors with internal amplification may have significant technological challenges. The planned fabrication of a prototype HPGe detector based on the results from this work can show if the existing technological limitations allow for the internal amplification of the signal in HPGe detectors.

CRediT authorship contribution statement

D. Maneuski: Writing – original draft, Software, Methodology, Investigation, Data curation, Conceptualization. **V. Gostilo:** Writing – review & editing, Supervision, Resources, Methodology, Investigation, Conceptualization.

Declaration of competing interest

The authors declare that they have no known competing financial interests or personal relationships that could have appeared to influence the work reported in this paper.

Data availability

Data will be made available on request.

Acknowledgements

This work has been supported by the STFC grant, UK ST/S000887/1. The authors thank A. Starostin (ITEPh) for many fruitful discussions of the challenges stated in this work. The authors acknowledge A. Sokolov and R. Nurgalejev (BSI) for their comprehensive discussion of the manufacturing aspects of the HPGe detectors. The authors are grateful to D. Spiteri (UofG) for helpful discussion on the manuscript and its content.

References

Bahcall, J., et al., 2001. Underground Science. Institute of Nuclear Physics, The University of Washington, pp. 1–36, http://www.sns.ias.edu/jnb/Laboratory/science.pdf, (Accessed on 01.08.2023).

Bruyneel, B., 2006. Characterization of segmented large volume, high purity germanium detectors. (Ph.D. thesis). Institut für Kernphysik, Köln, pp. 80–89, https://core.ac.uk/display/12009708.

Deng, Z., et al., 2018. An ultra-low noise cryogenic CMOS charge sensitive preamplifier for large volume point-contact HPGe detectors. J. Instrum. 13, P08019. http://dx.doi.org/10.1088/1748-0221/13/08/P08019.

Fan, H.Y., et al., 1954. Recombination and trapping of carriers in germanium. Physica 20 (7–12), 855–872. http://dx.doi.org/10.1016/S0031-8914(54)80198-4.

Farrell, R., et al., 1997. Advances in semiconductor photodetectors for scintillators. Nucl. Instrum. Methods A 387 (1–2), 194–198. http://dx.doi.org/10.1016/S0168-9002(96)00988-6.

Formaggio, J.A., Martoff, C.J., 2004. Backgrounds to sensitive experiments underground. Annu. Rev. Nucl. Part. Sci. 54 (1), 361–412. http://dx.doi.org/10.1146/annurev.nucl.54.070103.181248.

Gilchriese, M.G., et al., 2023. Planning the Future of US Particle Physics (Snowmass 2013): Underground Laboratory Capabilities. http://www.slac.stanford.edu/econf/C1307292/docs/Underground-7.pdf, (Accessed on 01.08.2023).

Gostilo, V., et al., 2001. Technological aspects of development of pixel and strip detectors based on CdTe and CdZnTe. Nucl. Instrum. Methods A 460 (1), 27–34. http://dx.doi.org/10.1016/S0168-9002(00)01091-3.

Gostilo, V., et al., 2002. Technological limitations and processing generated defects at the development of pixel and strip arrays. Nucl. Instrum. Methods A 487 (1–2), 13–18. http://dx.doi.org/10.1016/S0168-9002(02)00938-5.

Kang, Y., et al., 2009. Monolithic germanium/silicon avalanche photodiodes with 340 GHz gain–bandwidth product. Nat. Photon. 3 (1), 59. http://dx.doi.org/10.1038/nphoton.2008.247.

Knoll, G., 2000. Radiation Detection and Measurement, third ed. John Wiley and Sons, Inc., p. 802.

Laubenstein, M., et al., 2004. Underground measurements of radioactivity. Appl. Radiat. Isot. 61, 167–172. http://dx.doi.org/10.1016/j.apradiso.2004.03.039.

Lutz, G., 1999. Semiconductor Radiation Detectors, Device Physics. Springer, p. 353, https://link.springer.com/book/10.1007/978-3-540-71679-2.

Maneuski, D., et al., 2020. TCAD simulation studies of novel geometries for CZT ring-drift detectors. J. Phys. D: Appl. Phys. 53 (1), 015114. http://dx.doi.org/10.1088/1361-6463/ab49b1.

Mei, D.-M., et al., 2018. Direct detection of MeV-scale dark matter utilizing germanium internal amplification for the charge created by the ionization of impurities. Eur. Phys. J. C 78, 187. http://dx.doi.org/10.1140/epjc/s10052-018-5653-z.

Michel, J., et al., 2010. High-performance Ge-on-Si photodetectors. Nat. Photon. 4 (8), 527. http://dx.doi.org/10.1038/nphoton.2010.157.

Moffat, N., 2020. Low gain avalanche detectors for particle physics and synchrotron applications (Ph.D. thesis). University of Glasgow, https://theses.gla.ac.uk/81281/.

Moffat, N., Bates, R., 2021. Simulation of the small pixel effect contributing to a low fill factor for pixellated low gain avalanche detectors (LGAD). Nucl. Instrum. Methods A 1018, 165746. http://dx.doi.org/10.1016/j.nima.2021.165746.

Owens, A., 2019. Semiconductor Radiation Detectors. CRC Press, Taylor and Francis Group, p. 494. http://dx.doi.org/10.1201/b22251.

Pansart, J.P., 1997. Avalanche photodiodes for particle detection. Nucl. Instrum. Methods A 387 (1–2), 186–193. http://dx.doi.org/10.1016/S0168-9002(96)00987-4.

Pellegrini, G., et al., 2016. Recent technological developments on LGAD and iLGAD detectors for tracking and timing applications. Nucl. Instrum. Methods A 831, 24–28. http://dx.doi.org/10.1016/j.nima.2016.05.066.

Prakash, N., 2012. Dark Matter, Neutrinos and Our Solar System. World Scientific Publishing Co., p. 676. http://dx.doi.org/10.1142/7724.

Pratt, B., Friedman, F., 1966. Diffusion of Lithium into Ge and Si. J. Appl. Phys. 37 (4), 1893–1896. http://dx.doi.org/10.1063/1.1708620.

Pullia, A., et al., 2008. A cryogenic low-noise JFET-cmos preamplifier for the HPGe detectors of GERDA. In: IEEE Nuclear Science Symposium Conference Record. Nuclear Science Symposium. pp. 2056–2060. http://dx.doi.org/10.1109/NSSMIC.2008.4774881.

Renker, D., Lorenz, E., 2009. Advances in solid state photon detectors. J. Instrum. 4, P04004. http://dx.doi.org/10.1088/1748-0221/4/04/P04004.

Schlesinger, T.E., James, R.B., 1995. Semiconductors for Room Temperature Nuclear Detector Applications. Semiconductors and Semimetals. Vol.43, Academic Press, p. 606, https://www.sciencedirect.com/bookseries/semiconductors-and-semimetals/vol/43.

Starostin, A., Beda, A., 2000. Germanium detector with an internal amplification for investigating rare processes. Phys. Atomic Nucl. 63 (7), 1297–1300. http://dx.doi.org/10.1134/1.855787.

Synopsys, 2023. Synopsys TCAD version 2017. Web page, https://www.synopsys.com/silicon/tcad.html, (Accessed on 24.11.2023).

Tapan, I., et al., 1997. Avalanche photodiodes as proportional particle detectors. Nucl. Instrum. Methods A 388 (1–2), 79–90. http://dx.doi.org/10.1016/S0168-9002(97)00316-1.